

Supporting Information for

Stoichiometric Control: 8- and 10-coordinate Ln(hfac)₃(bpy) and Ln(hfac)₃(bpy)₂ Complexes of the Early Lanthanides La – Sm

Elisabeth M. Fatila,^{a,b*} Adam C. Maahs,^a Erin E. Hetherington,^a Brandon J. Cooper,^b Riley E. Cooper,^b Nick N. Daanen,^d Michael Jennings,^c Sara E. Skrabalak,^d and Kathryn E. Preuss^{a*}

^a Department of Chemistry, University of Guelph, Guelph, ON, N1G 2W1, Canada

^b Department of Chemistry, Louisiana Tech. University, Ruston, LA, 71272, USA

^c FreeLance Crystallography, 185 Chelsea Ave. London, ON, N6J 3J5, Canada

^d Department of Chemistry, Indiana University Bloomington, Bloomington, IN, 47405, USA

SI. 1:1 Mechanochemical Reaction of Ln(hfac)₃(H₂O)₃ and bpy

La(hfac)₃(H₂O)₃ and 1 eq. bpy: La(hfac)₃(H₂O)₃ was ground into a fine powder (0.2009 g, 0.2462 mmol) and added to 2,2'-bipyridine (0.0394 g, 0.252 mmol). The mixture was ground together in an agate mortar and pestle for approximately 30 minutes. The material was collected and analyzed by IR and DSC. DSC phase transitions: 58-69 °C. IR (KBr, Nujol) ν /cm⁻¹: **3510**(mw,br), 3407(mw,br), 1653(s), 1600(w), 1577(w), 1566(w,br), 1558(w), 1539(w,br), 1507(mw), 1494(mw,br), 1465(m,br), 1457(m), 1438(mw,sh), 1348(vw), 1320(w), 1318(vw), 1312(vw), 1253(s,br), 1205(s,br), 1199(s,br), 1150(s,sh), 1144(s,br), 1096(mw), 1064(w), 1046(vw), 1043(vw), 1025(w), 1012(w), 1008(mw), 1003(vw,sh), 977(vw), 952(vw), 949(vw), 807(ms), 804(ms), **797**(ms), **793**(ms), 766(m), 754(ms), 740(ms), 721(mw), 670(m,sh), 668(ms), 660(s), 653(mw), 644(w), 640(mw), 625(vw), 622(w).

Ce(hfac)₃(H₂O)₃ and 1 eq. bpy: Ce(hfac)₃(H₂O)₃ was ground into a fine powder (0.2516 g, 0.3086 mmol) and added to 2,2'-bipyridine (0.0504 g, 0.323 mmol). The mixture was ground together in an agate mortar and pestle for approximately 30 minutes. The material was collected and analyzed by IR and DSC. DSC phase transitions: broad centered at 70°C with two smaller transitions ranging from 88 – 100 °C. IR (KBr, Nujol) ν /cm⁻¹: **3630**(mw), **3506**(mw,br), 3405(mw,br), 3182(w), 3144(w), 1655(s), 1600(mw), 1579(mw), 1560(mw), 1532(m), 1510(m), 1494(m,sh), 1465(s,br), 1457(m), 1365(m), 1350(w), 1320(w),

1311(vw), 1254(s,br), 1207(s,br), 1140(s,br), 1097(ms), 1064(mw), 1046(w), 1024(w), 1012(mw), 1008(mw), 969(vw), 950(w), 918(vw), 889(vw), 805(m), **799**(ms), **793**(ms,sh), 766(mw), 761(ms), 740(ms), 721(mw), 670(m,sh), 670(mw), 660(s), 652(mw), 644(w), 640(w), 625(vw), 622(w).

Pr(hfac)₃(H₂O)₃ and 1 eq. bpy: Pr(hfac)₃(H₂O)₃ was ground into a fine powder (0.2513 g, 0.3086 mmol) and added to 2,2'-bipyridine (0.0506 g, 0.324 mmol). The mixture was ground together in an agate mortar and pestle for approximately 30 minutes. The material was collected and analyzed by IR and DSC. DSC phase transitions: broad centered at 70°C with three smaller transitions ranging from 80 – 88 °C, 95 – 99 °C, 107 – 118 °C. IR (KBr, Nujol) ν /cm⁻¹: **3506**(w,br), 3397(w,br), 3313(w,br), 3143(w), 1654(s), 1600(mw), 1578(mw), 1567(w), 1558(mw) 1533(m), 1496(m,br), 1476(ms), 1465(s,br), 1443(m), 1377(mw), 1348(w), 1321(w), 1311(vw), 1254(s,br), 1207(s), 1197(s), 1143(s,br), 1100(m), 1065(vw), 1044(vw), 1025(w), 1013(mw), 1008(mw), 969(vw), 951(vw), 908(vw), 807(m), **798**(m), 766(m), 760(m), 740(m), 722(w), 670(mw,sh), 661(ms), 653(w), 644(w), 640(w), 625(vw), 622(w).

Nd(hfac)₃(H₂O)₃ and 1 eq. bpy: Nd(hfac)₃(H₂O)₃ was ground into a fine powder (0.2510 g, 0.3132 mmol) and added to 2,2'-bipyridine (0.0497 g, 0.318 mmol). The mixture was ground together in an agate mortar and pestle for approximately 30 minutes. The material was collected and analyzed by IR and DSC. DSC phase transitions: broad centered at 70°C with two smaller transitions centered at approximately 80 and 87 °C. Two other transitions are noted from 98 – 105 °C and 117 – 124 °C. IR (KBr, Nujol) ν /cm⁻¹: **3502**(vw,br), 3387(w,br), 3298(w,br), 3141(vw), 1664(s), 1649(s), 1605(mw), 1599(mw), 1578(mw), 1560(mw) 1534(m), 1509(m), 1495(m,br), 1478(ms), 1462(ms,br), 1443(m), 1377(mw), 1366(w), 1351(w), 1321(w), 1311(vw), 1256(s,br), 1208(s), 1145(s,br), 1100(m), 1065(vw), 1044(vw), 1025(w), 1015(mw), 1008(w), 989(vw), 970(vw), 950(w), 909(w), 804(m), **799**(m), **797**(m), 765(m,sh), 763(m), 739(m), 721(w), 665(mw,sh), 660(ms), 653(w), 647(w), 633(vw,br), 628(vw).

S2. IR, PXRD and DSC Data for Mechanochemical Reactions and Syntheses

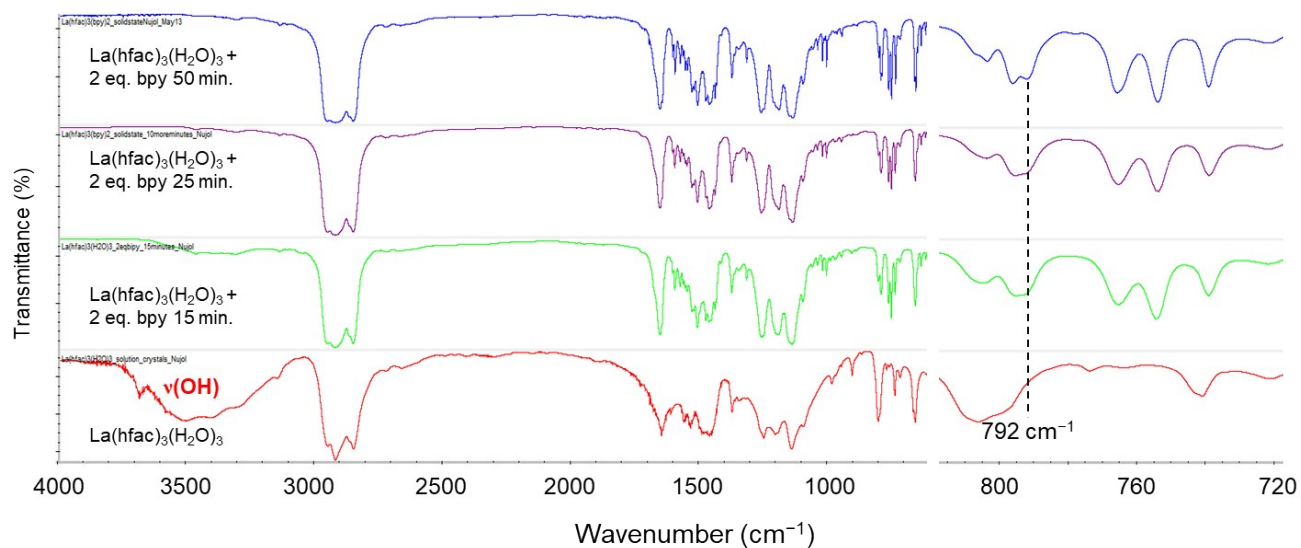


Figure S1. FT-IR spectra following the mechanochemical synthesis of $\text{La}(\text{hfac})_3(\text{bpy})_2$ from $\text{La}(\text{hfac})_3(\text{H}_2\text{O})_3$; the absorption at 792 cm^{-1} indicates formation of 10-coordinate complex.

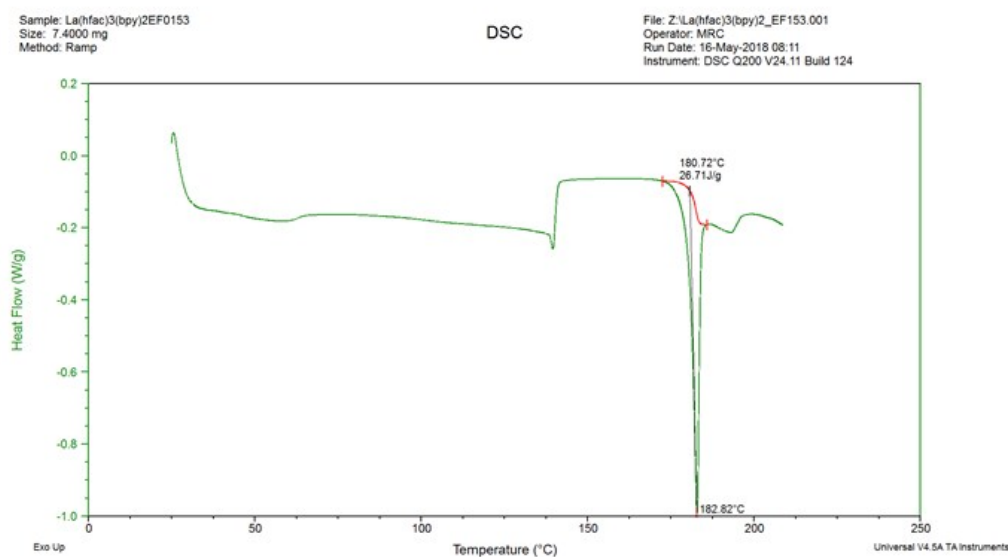


Figure S2. DSC of $\text{La}(\text{hfac})_3(\text{bpy})_2$ prepared from $\text{La}(\text{hfac})_3(\text{H}_2\text{O})_3$ by mechanochemical synthesis ($T_i = 25^{\circ}\text{C}$ heating $25^{\circ}\text{C}/\text{min}$ to 140°C , heating $5^{\circ}\text{C}/\text{min}$ from 140°C to 215°C)

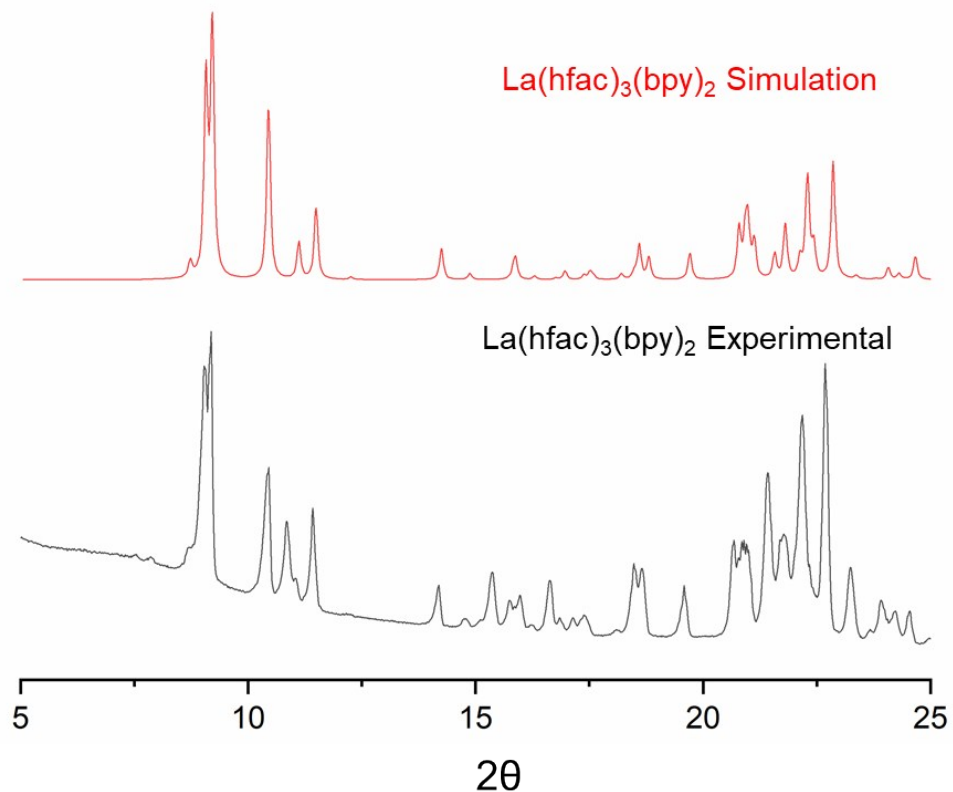


Figure S3. (top) PXRD simulation of $\text{La}(\text{hfac})_3(\text{bpy})_2$ obtained from crystal structure (collected at 213(2) K) and (bottom) experimental PXRD of $\text{La}(\text{hfac})_3(\text{bpy})_2$ from mechanochemical synthesis collected at 298 K

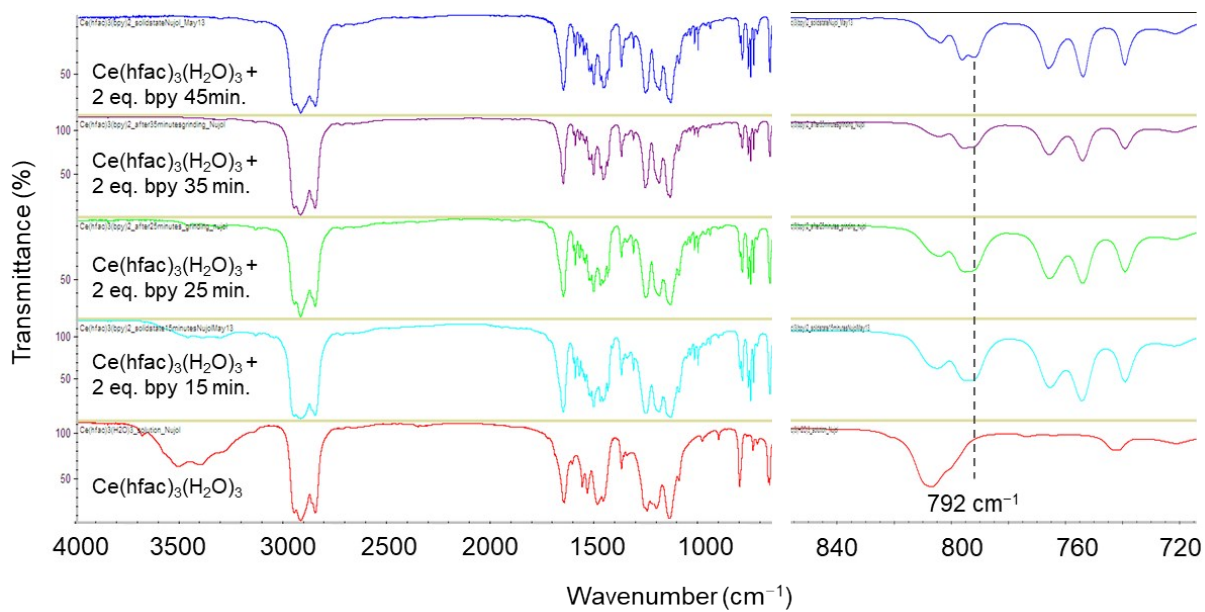


Figure S4. FT-IR spectra following the mechanochemical synthesis of $\text{Ce}(\text{hfac})_3(\text{bpy})_2$ from $\text{Ce}(\text{hfac})_3(\text{H}_2\text{O})_3$

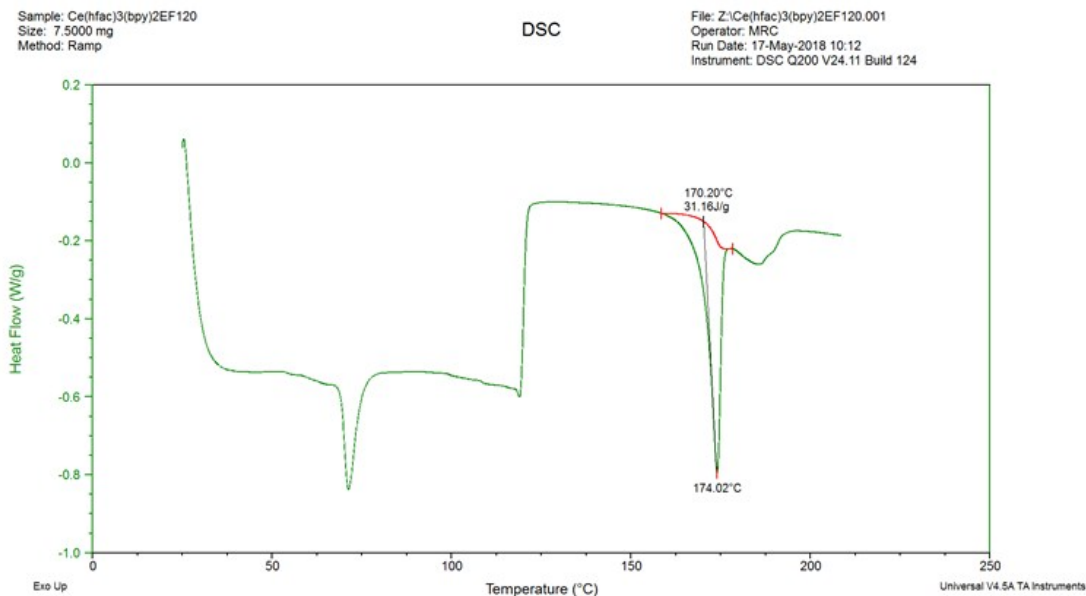


Figure S5. DSC of Ce(hfac)₃(bpy)₂ prepared from Ce(hfac)₃(H₂O)₃ by mechanochemical synthesis ($T_i = 25\text{ }^\circ\text{C}$ heating $25\text{ }^\circ\text{C}/\text{min}$ to $120\text{ }^\circ\text{C}$, heating $5\text{ }^\circ\text{C}/\text{min}$ from $120\text{ }^\circ\text{C}$ to $210\text{ }^\circ\text{C}$)

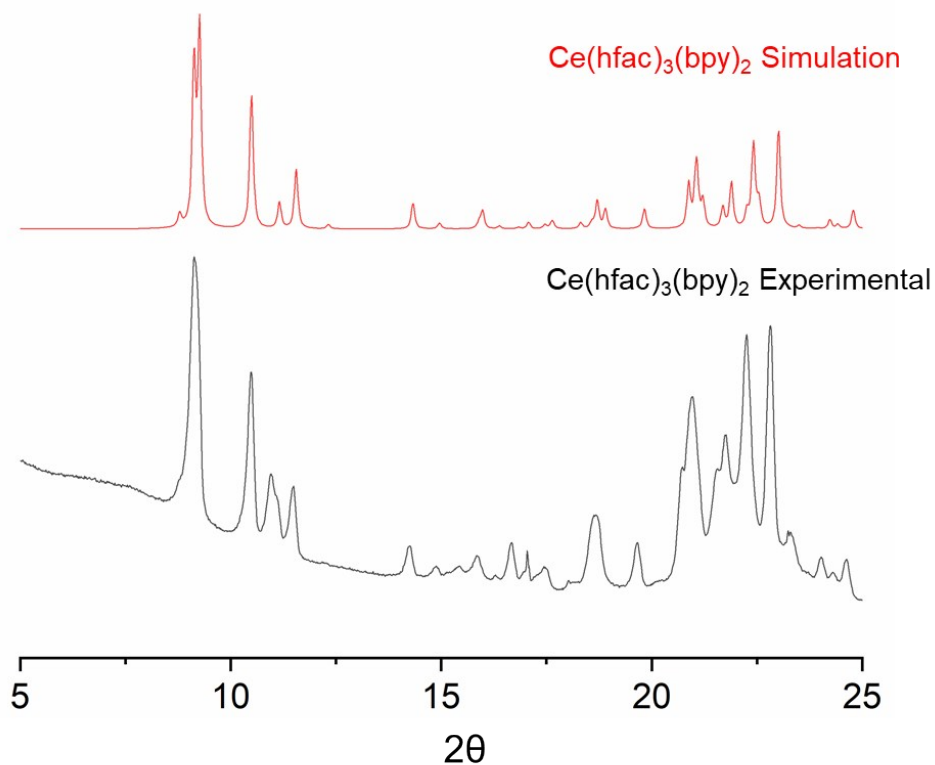


Figure S6. (top) PXRD simulation of Ce(hfac)₃(bpy)₂ obtained from crystal structure (collected at $150(2)\text{ K}$) and (bottom) experimental PXRD of Ce(hfac)₃(bpy)₂ from mechanochemical synthesis collected at 298 K

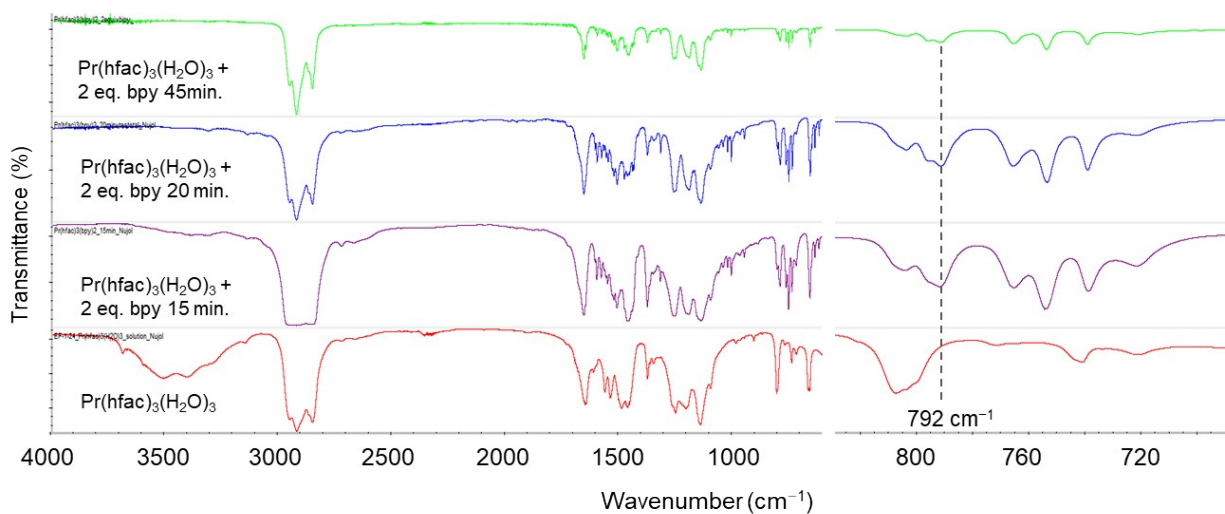


Figure S7. FT-IR spectra following the mechanochemical synthesis of $\text{Pr}(\text{hfac})_3(\text{bpy})_2$ from $\text{Pr}(\text{hfac})_3(\text{H}_2\text{O})_3$

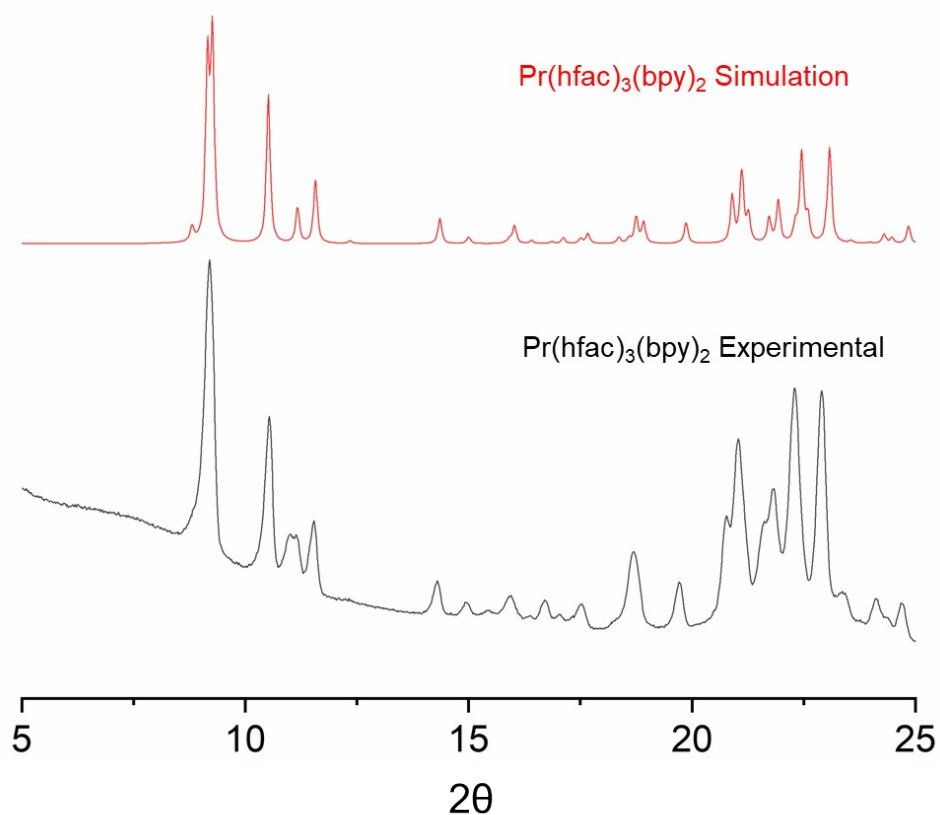


Figure S8. (top) PXR D comparison from simulation of $\text{Pr}(\text{hfac})_3(\text{bpy})_2$ obtained from crystal structure (collected at 150(2) K) and (bottom) experimental PXR D of $\text{Pr}(\text{hfac})_3(\text{bpy})_2$ from mechanochemical synthesis collected at 298 K

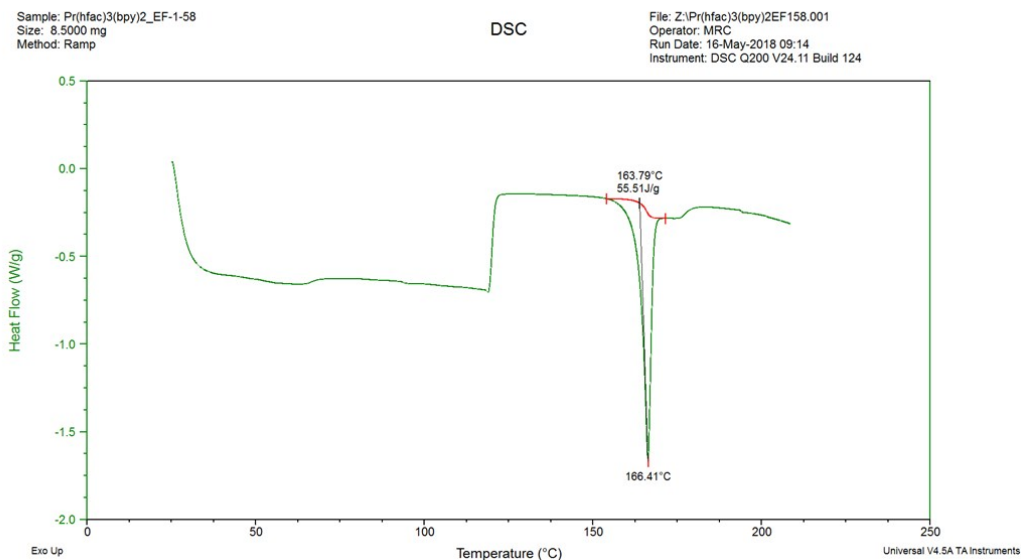


Figure S9. DSC of Pr(hfac)₃(bpy)₂ prepared from Pr(hfac)₃(H₂O)₃ by mechanochemical synthesis ($T_i = 25$ °C heating 25 °C/min to 120 °C, heating 5 °C/min from 120 °C to 215 °C)

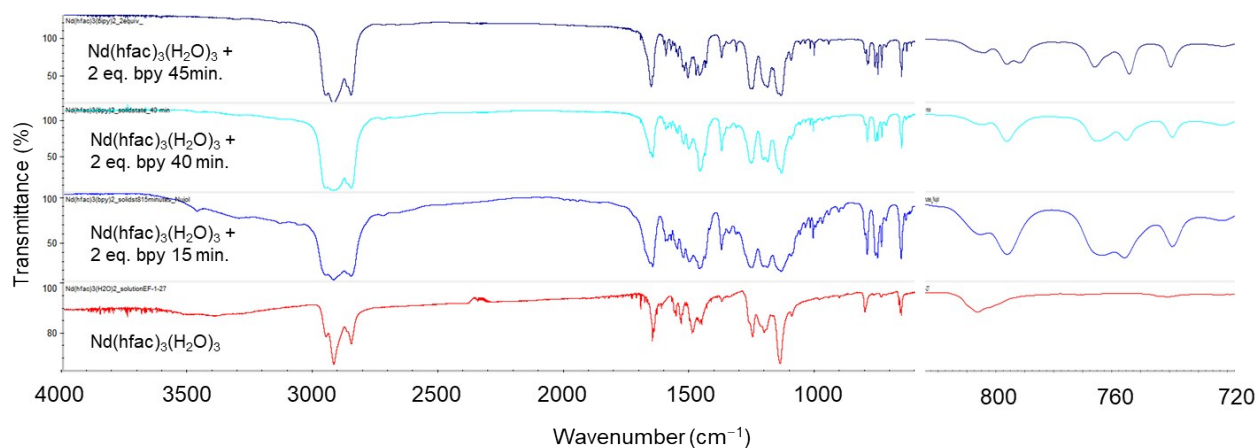


Figure S10. FT-IR spectra following the mechanochemical synthesis of Nd(hfac)₃(bpy)₂ from Nd(hfac)₃(H₂O)₃

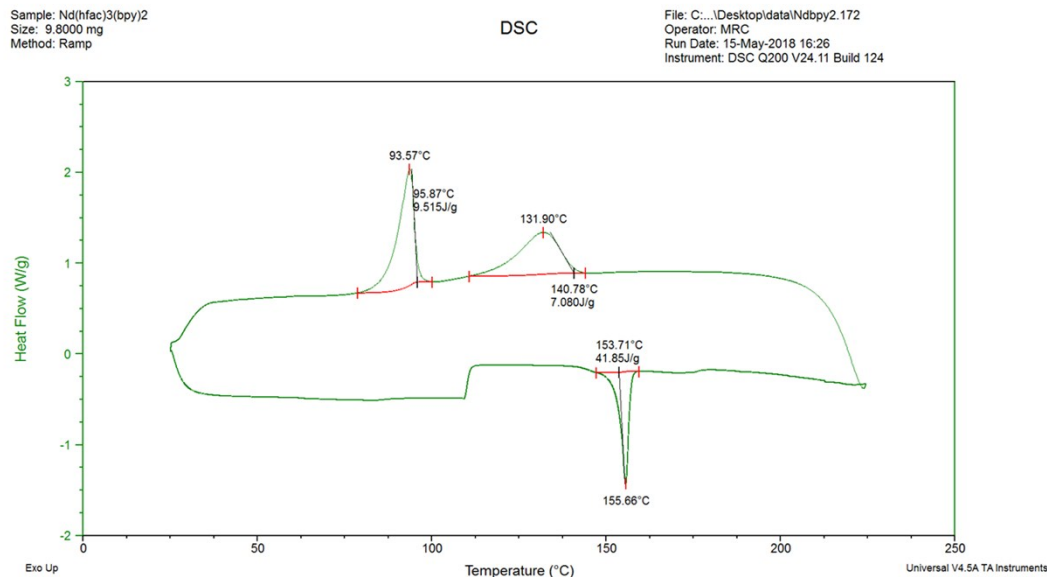


Figure S11. DSC of Nd(hfac)₃(bpy)₂ prepared from Nd(hfac)₃(H₂O)₃ by mechanochemical synthesis ($T_i = 25\text{ }^\circ\text{C}$ heating $25\text{ }^\circ\text{C}/\text{min}$ to $110\text{ }^\circ\text{C}$, heating $5\text{ }^\circ\text{C}/\text{min}$ from $110\text{ }^\circ\text{C}$ to $225\text{ }^\circ\text{C}$, cooling $5\text{ }^\circ\text{C}/\text{min}$ from $225\text{ }^\circ\text{C}$ to $25\text{ }^\circ\text{C}$)

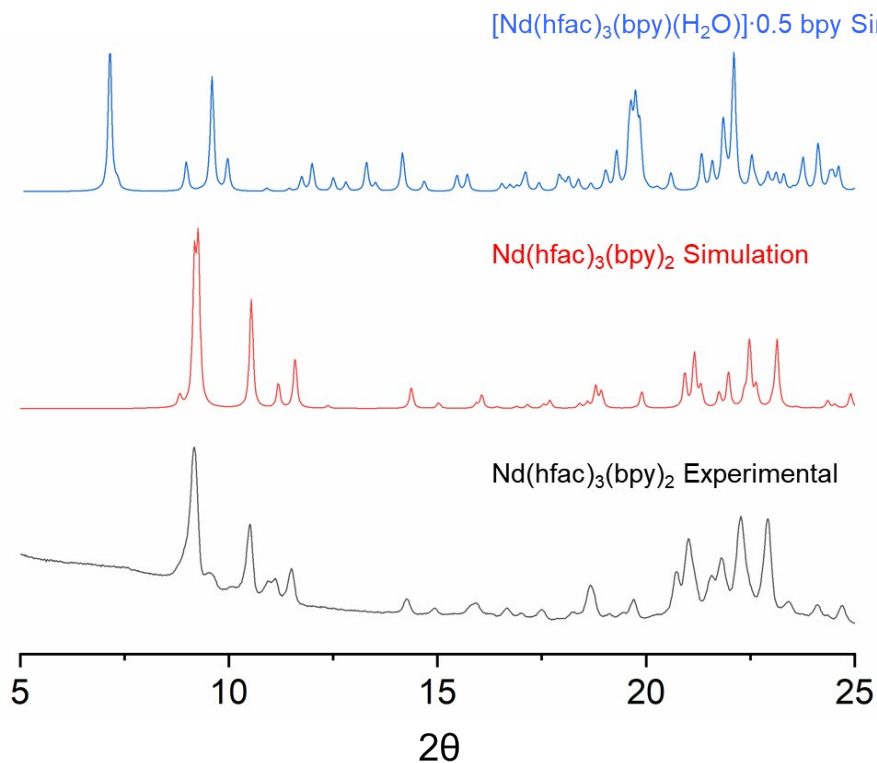


Figure S12. PXR D comparison from simulation of (top) [Nd(hfac)₃(bpy)(H₂O)]·0.5(bpy) obtained from crystal structure (collected at 150(2) K) and (middle) Nd(hfac)₃(bpy)₂ obtained from crystal structure

collected at 150 K and (bottom) experimental PXRD of $\text{Nd}(\text{hfac})_3(\text{bpy})_2$ from mechanochemical synthesis collected at 298 K.

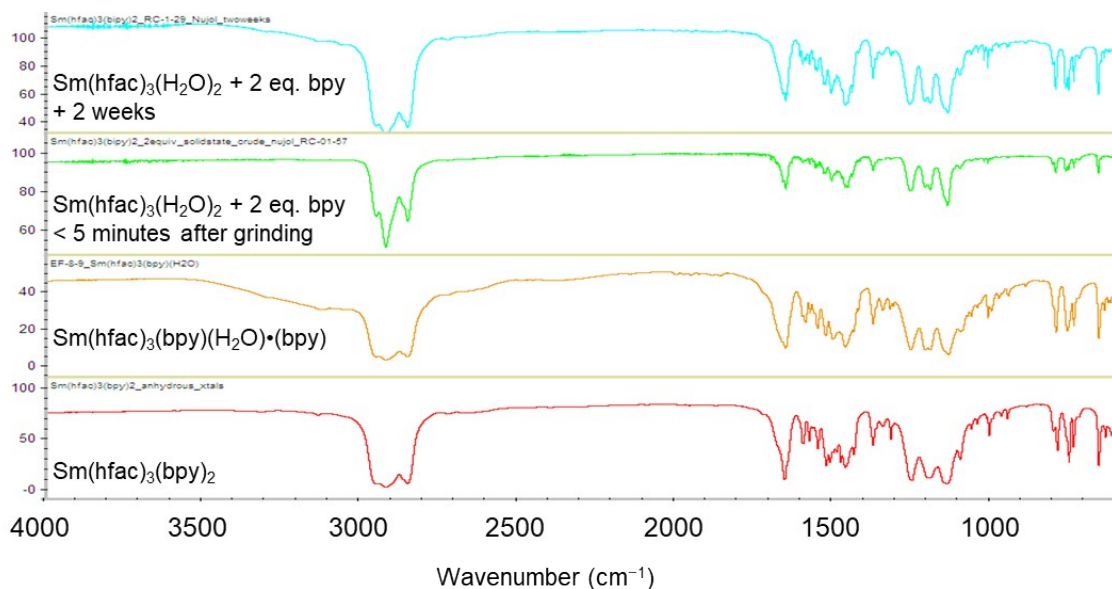


Figure S13. FT-IR spectra of mechanochemical attempt at making $\text{Sm}(\text{hfac})_3(\text{bpy})_2$ in air compared to hydrated $[\text{Sm}(\text{hfac})_3(\text{bpy})(\text{H}_2\text{O})] \cdot \text{bpy}$

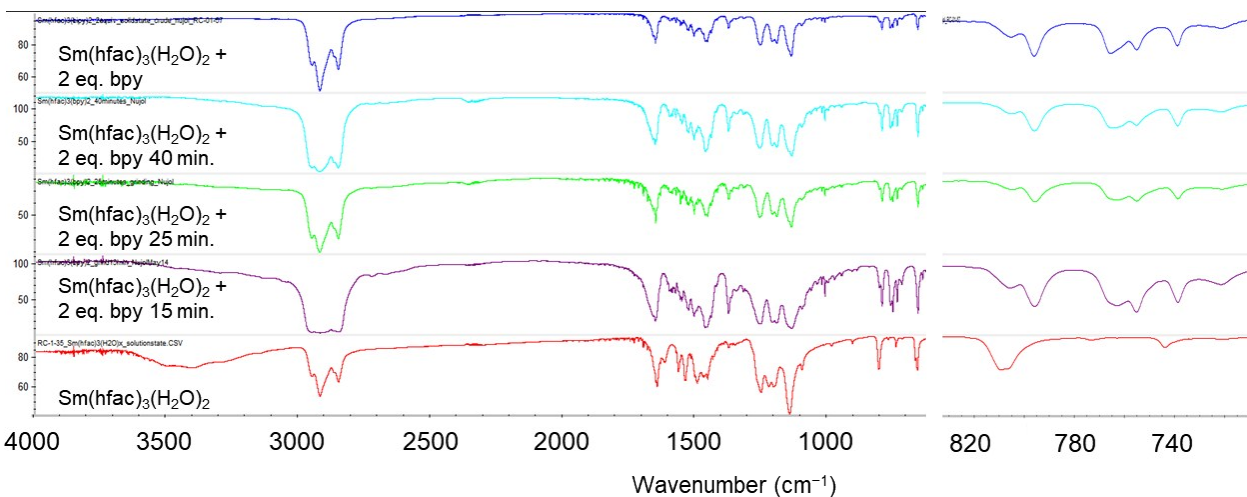


Figure S14. FT-IR spectra of mechanochemical attempt at making $\text{Sm}(\text{hfac})_3(\text{bpy})_2$ from $\text{Sm}(\text{hfac})_3(\text{H}_2\text{O})_2$

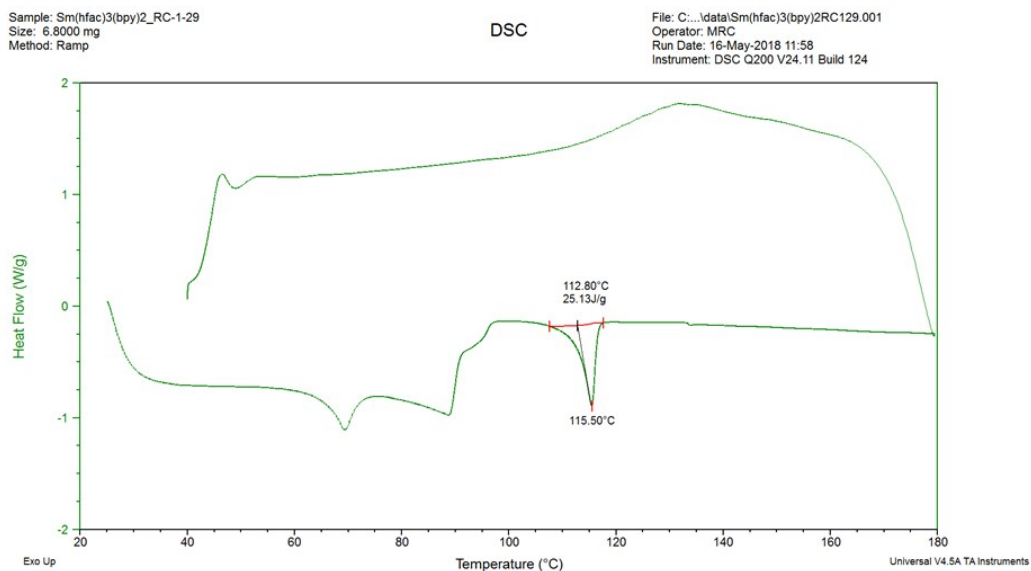


Figure S15. DSC of product from mechanochemical reaction of Sm(hfac)₃(H₂O)₂ and 2 equivalents of bpy ($T_i = 25\text{ }^\circ\text{C}$ heating $25\text{ }^\circ\text{C}/\text{min}$ to $90\text{ }^\circ\text{C}$, heating $5\text{ }^\circ\text{C}/\text{min}$ from $90\text{ }^\circ\text{C}$ to $180\text{ }^\circ\text{C}$, cooling $5\text{ }^\circ\text{C}/\text{min}$ to $40\text{ }^\circ\text{C}$)

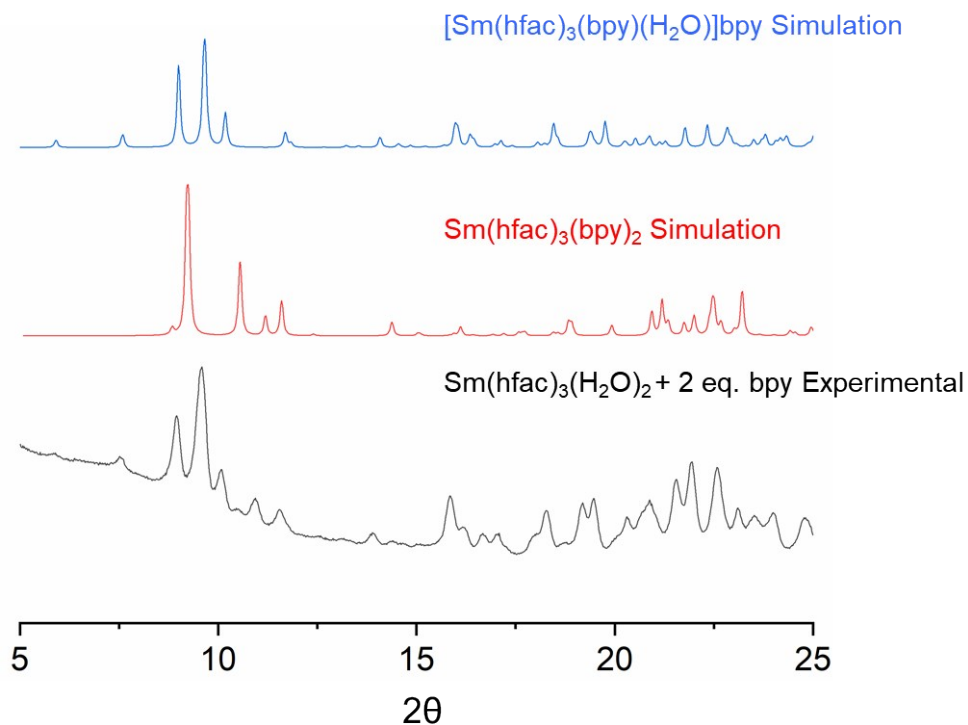


Figure S16. PXRD comparison from simulation of (top) [Sm(hfac)₃(bpy)(H₂O)]·bpy obtained from crystal structure (collected at 150(2) K) and (middle) Sm(hfac)₃(bpy)₂ obtained from crystal structure collected at 150 K and (bottom) experimental PXRD of Sm(hfac)₃(H₂O)₂ + 2 eq. bpy from mechanochemical reaction collected at 298 K

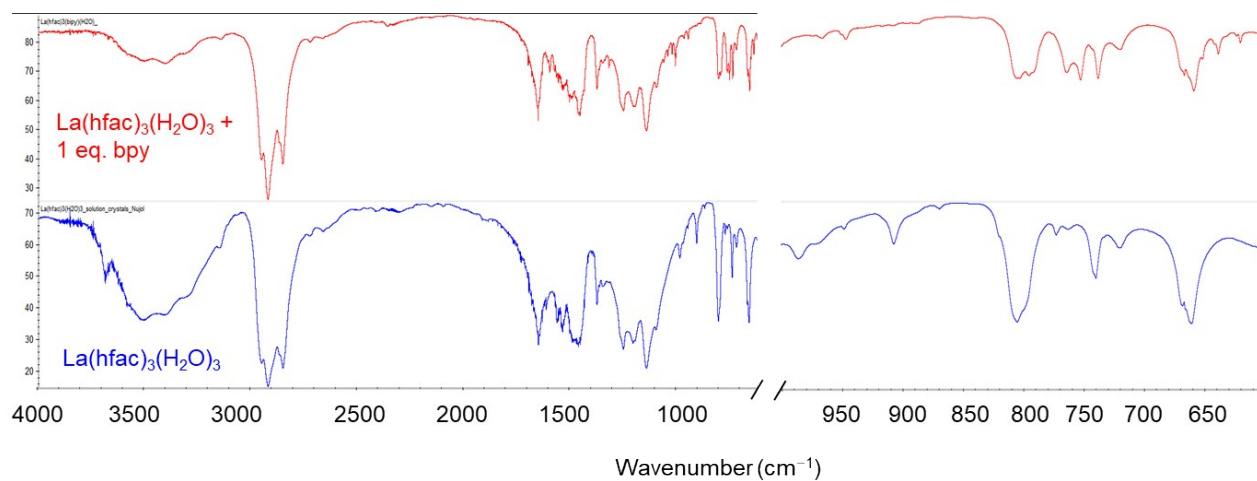


Figure S17. FT-IR spectra of mechanochemical reaction of $\text{La}(\text{hfac})_3(\text{H}_2\text{O})_3$ and 1 eq. of 2,2'-bipyridine

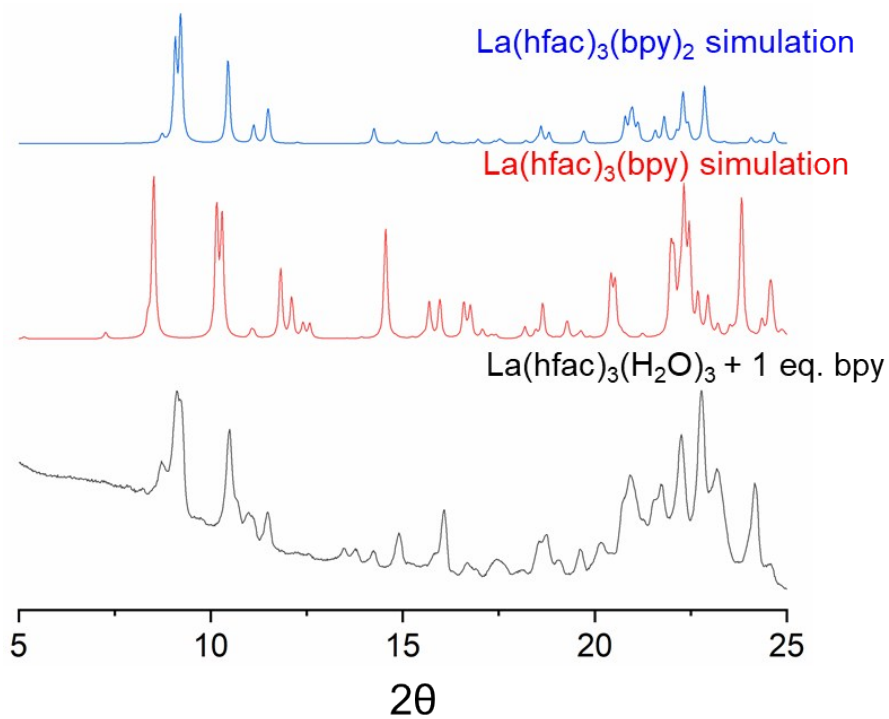


Figure S18. Simulated PXRD spectra of (top) $\text{La}(\text{hfac})_3(\text{bpy})_2$ and (middle) $\text{La}(\text{hfac})_3(\text{bpy})$ both obtained from single crystal data collected at 213 K and 150 K respectively and (bottom) PXRD spectrum of crude reaction of $\text{La}(\text{hfac})_3(\text{H}_2\text{O})_3$ and 1 eq. of 2,2'-bipyridine

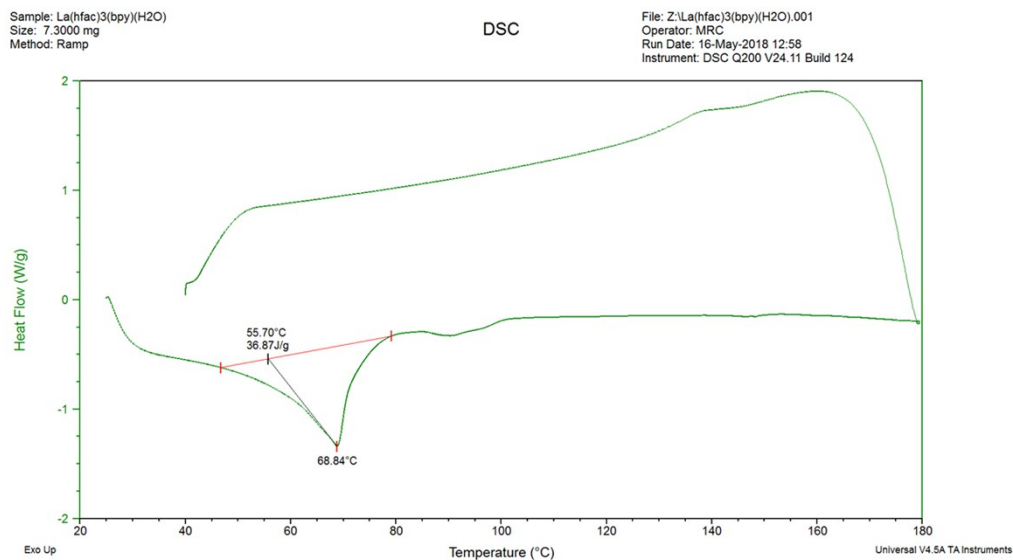


Figure S19. DSC of crude material from mechanochemical reaction of La(hfac)₃(H₂O)₃ and 1 eq. of 2,2'-bipyridine ($T_i = 25\text{ }^\circ\text{C}$ heating $25\text{ }^\circ\text{C}/\text{min}$ to $70\text{ }^\circ\text{C}$, heating $5\text{ }^\circ\text{C}/\text{min}$ from $70\text{ }^\circ\text{C}$ to $180\text{ }^\circ\text{C}$, cooling $5\text{ }^\circ\text{C}/\text{min}$ to $40\text{ }^\circ\text{C}$)

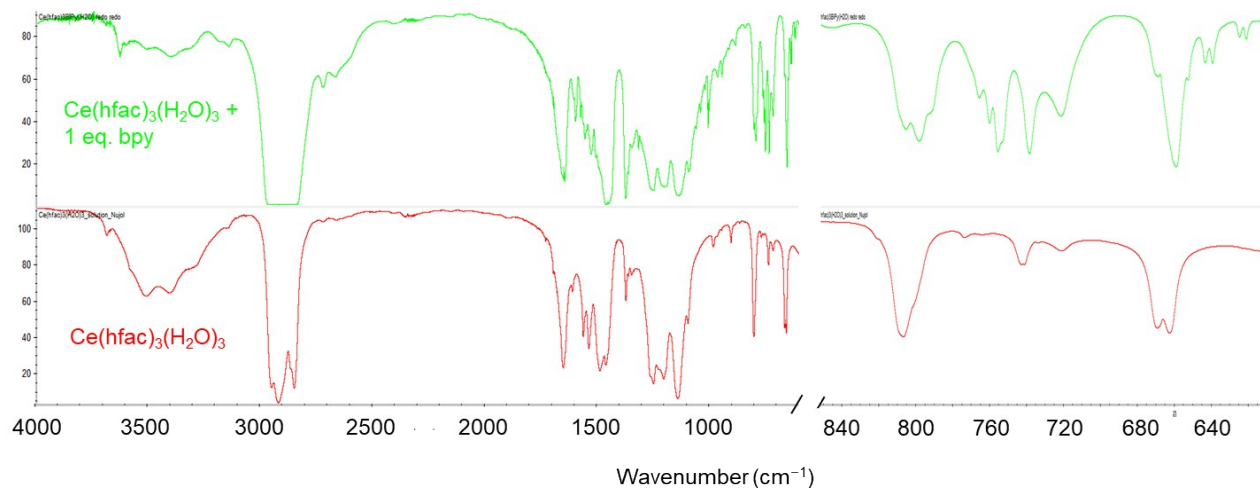


Figure S20. FT-IR spectra of mechanochemical reaction of Ce(hfac)₃(H₂O)₃ and 1 eq. of 2,2'-bipyridine

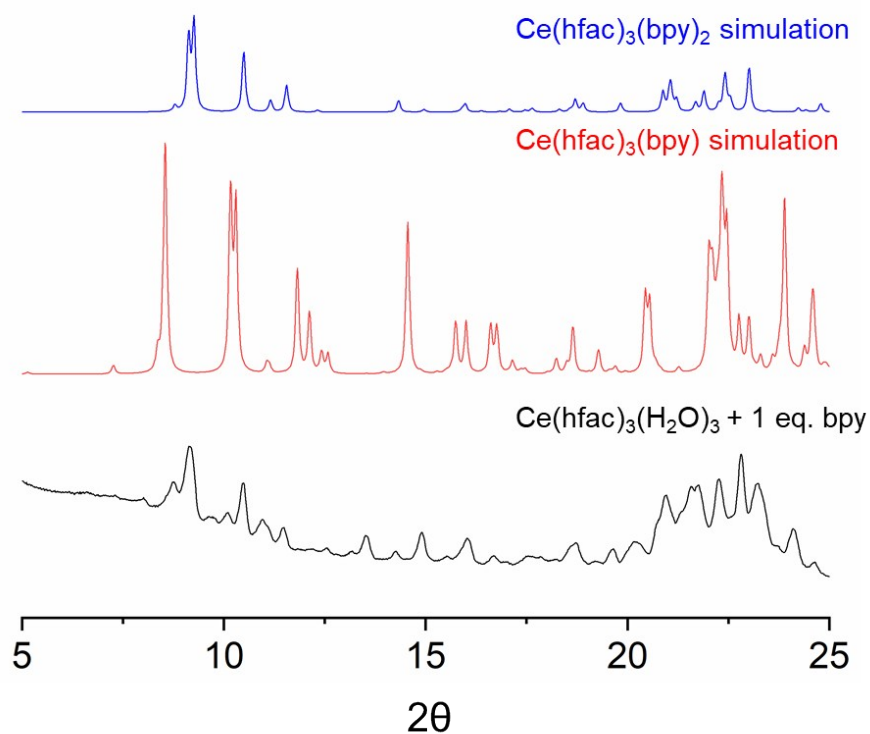


Figure S21. Simulated PXRD spectra of (top) $\text{Ce}(\text{hfac})_3(\text{bpy})_2$ and (middle) $\text{Ce}(\text{hfac})_3(\text{bpy})$ both obtained from single crystal data collected at 150 K and (bottom) PXRD spectrum of crude reaction of $\text{Ce}(\text{hfac})_3(\text{H}_2\text{O})_3$ and 1 eq. of 2,2'-bipyridine

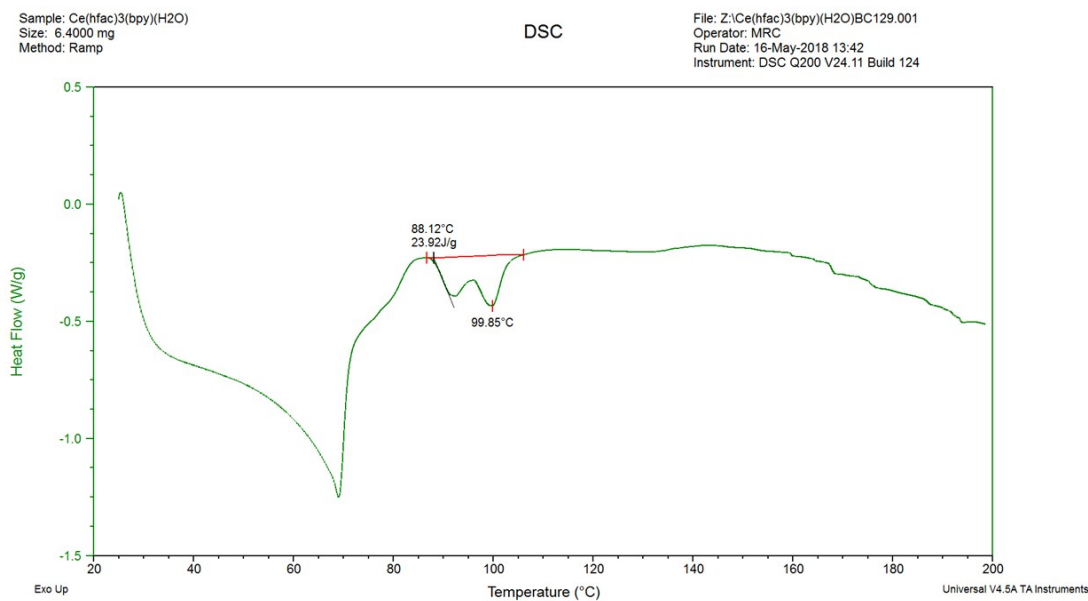


Figure S22. DSC of crude material from mechanochemical reaction of $\text{Ce}(\text{hfac})_3(\text{H}_2\text{O})_3$ and 1 eq. of 2,2'-bipyridine ($T_1 = 25^\circ\text{C}$ heating $25^\circ\text{C}/\text{min}$ to 70°C , heating $5^\circ\text{C}/\text{min}$ from 70°C to 200°C)

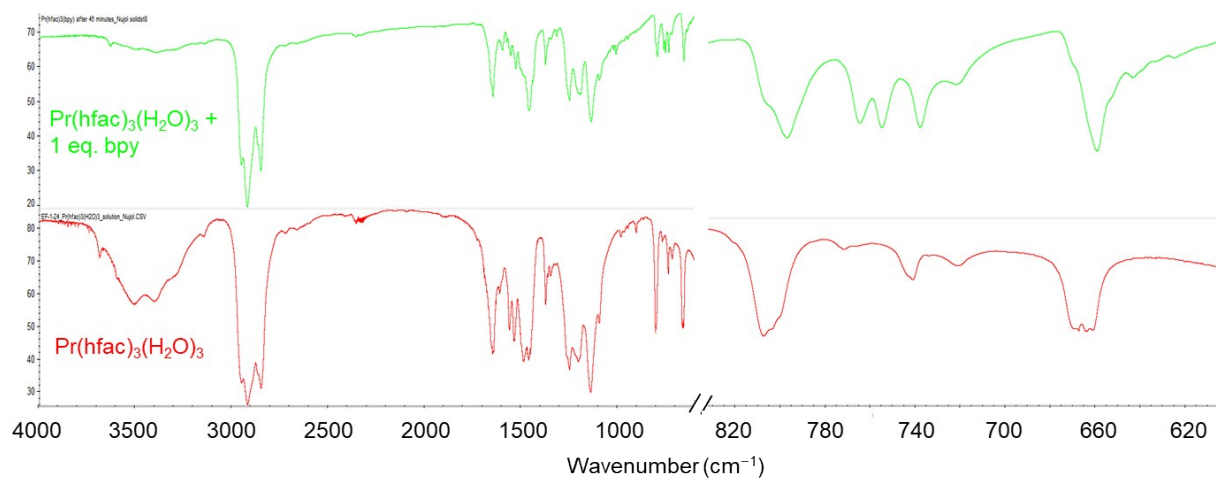


Figure S23. FT-IR spectra of mechanochemical reaction of Pr(hfac)₃(H₂O)₃ and 1 eq. of 2,2'-bipyridine

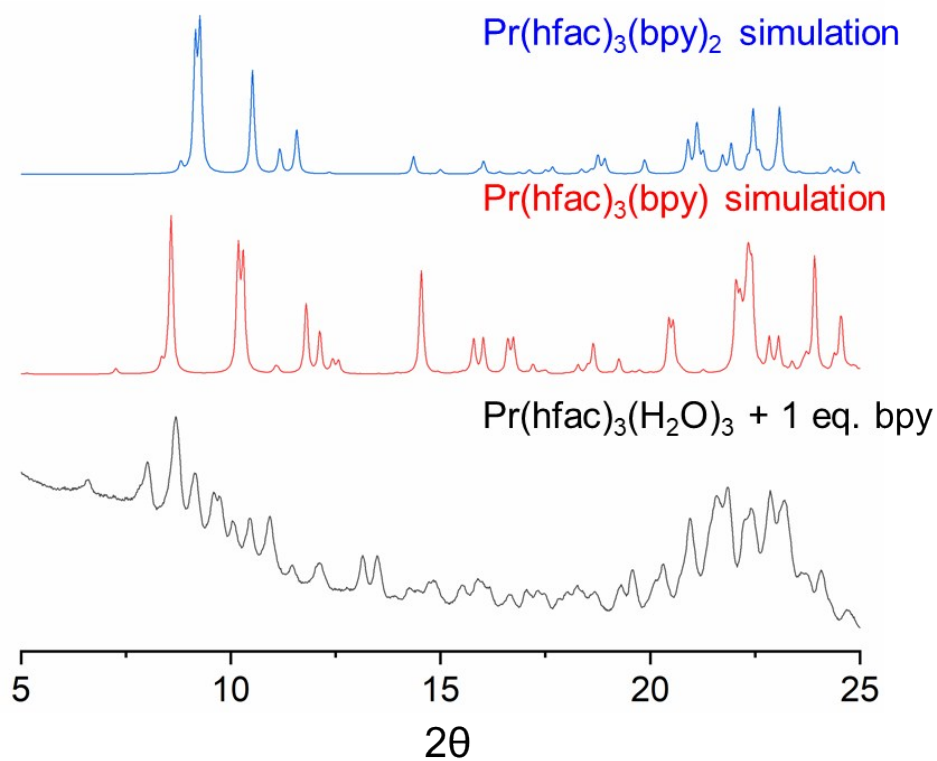


Figure S24. Simulated PXRD spectra of (top) Pr(hfac)₃(bpy)₂ and (middle) Pr(hfac)₃(bpy) both obtained from single crystal data collected at 150 K respectively and (bottom) PXRD spectrum of crude mechanochemical reaction of Pr(hfac)₃(H₂O)₃ and 1 eq. of 2,2'-bipyridine

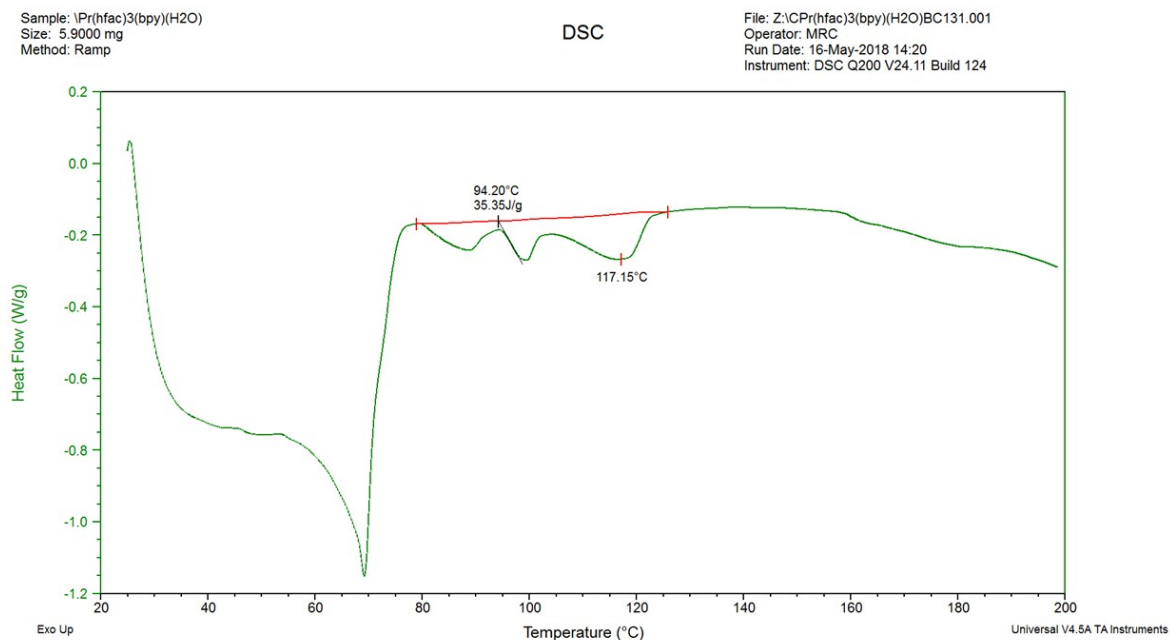


Figure S25. DSC of crude material from mechanochemical reaction of $\text{Pr}(\text{hfac})_3(\text{H}_2\text{O})_3$ and 1 eq. of 2,2'-bipyridine ($T_i = 25^\circ\text{C}$ heating $25^\circ\text{C}/\text{min}$ to 70°C , heating $5^\circ\text{C}/\text{min}$ from 70°C to 200°C)

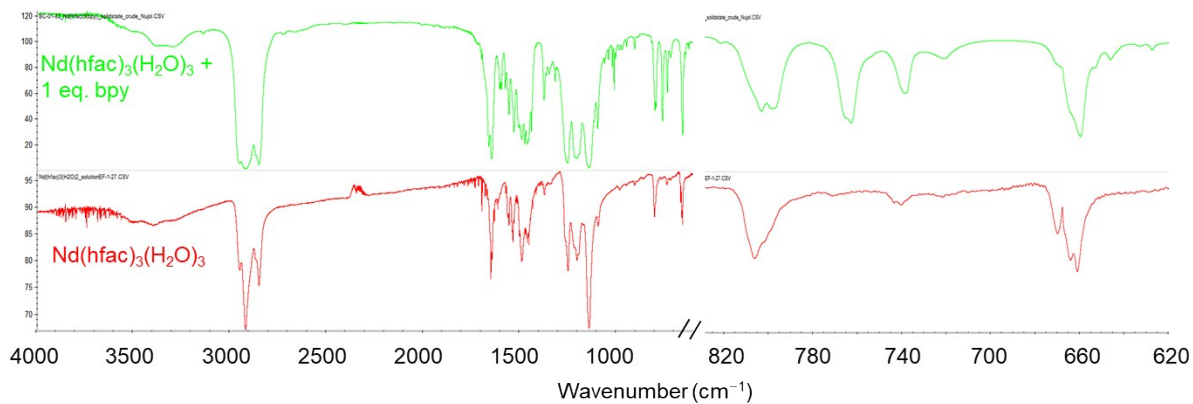


Figure S26. FT-IR spectra of mechanochemical reaction of $\text{Nd}(\text{hfac})_3(\text{H}_2\text{O})_3$ and 1 eq. of 2,2'-bipyridine

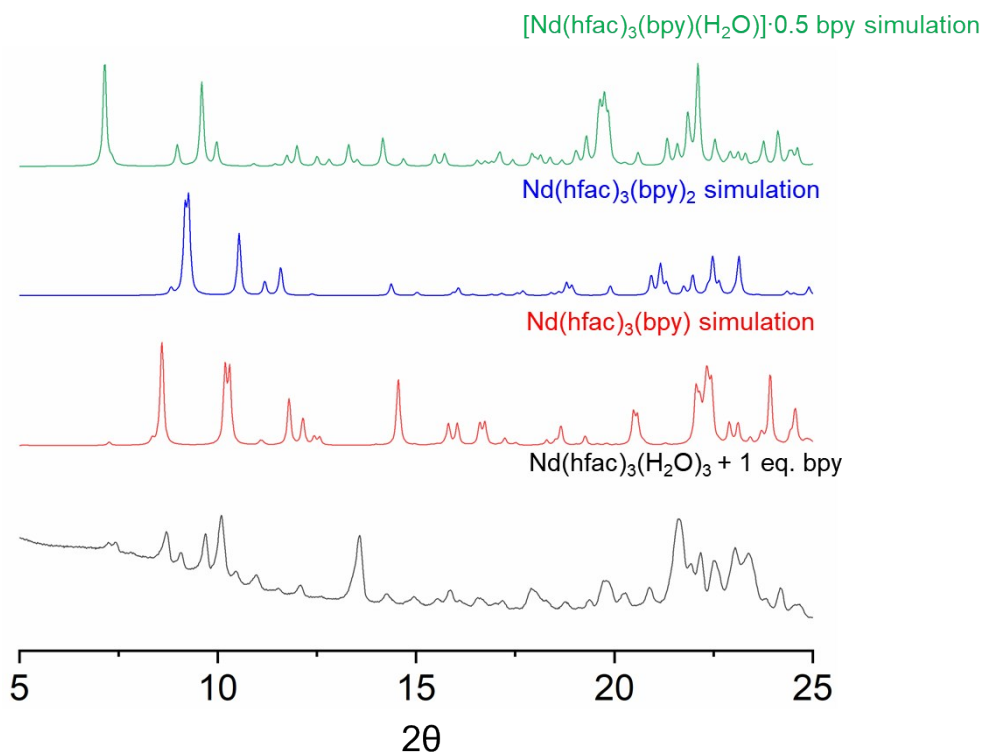


Figure S27. Simulated PXRD spectra of (top) $[\text{Nd}(\text{hfac})_3(\text{bpy})(\text{H}_2\text{O})]\cdot 0.5 \text{ bpy}$, (second from top) $\text{Nd}(\text{hfac})_3(\text{bpy})_2$ and (third from top) $\text{Nd}(\text{hfac})_3(\text{bpy})$ obtained from single crystal data collected at 150 K respectively, and (bottom) PXRD spectrum of crude reaction of $\text{Nd}(\text{hfac})_3(\text{H}_2\text{O})_3$ and 1 eq. of 2,2'-bipyridine.

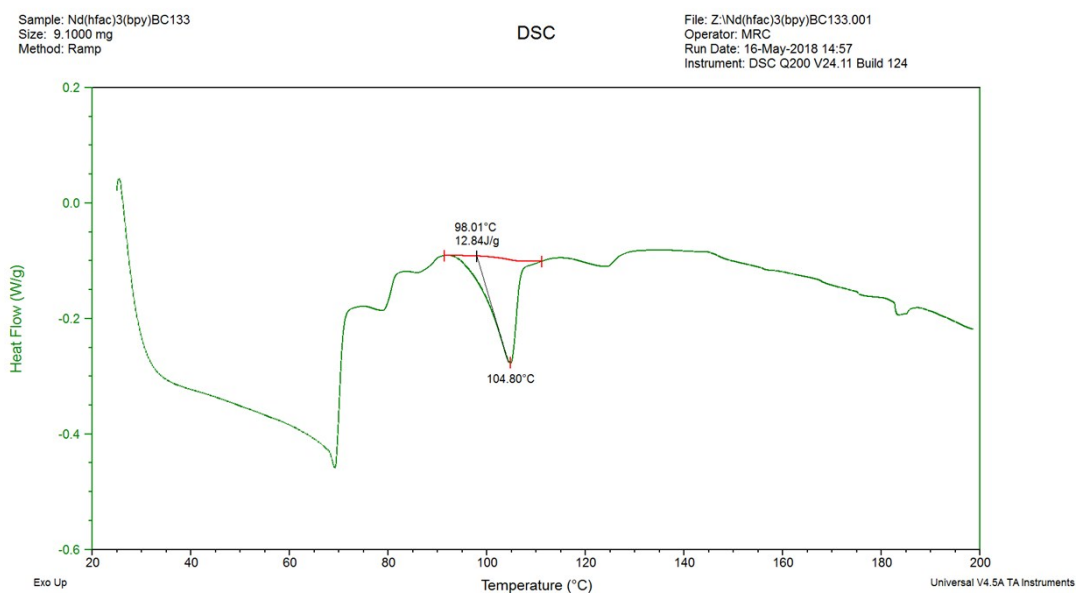


Figure S28. DSC of crude material from mechanochemical reaction of $\text{Nd}(\text{hfac})_3(\text{H}_2\text{O})_3$ and 1 eq. of 2,2'-bipyridine ($T_i = 25^\circ\text{C}$ heating $25^\circ\text{C}/\text{min}$ to 70°C , heating $5^\circ\text{C}/\text{min}$ from 70°C to 200°C)

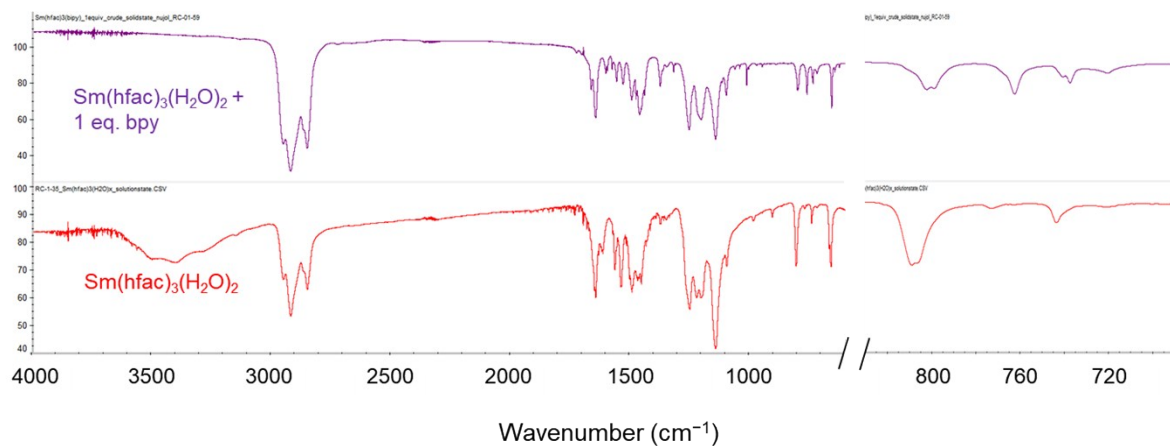


Figure S29. FT-IR spectra of mechanochemical reaction of $\text{Sm}(\text{hfac})_3(\text{H}_2\text{O})_2$ and 1 eq. of 2,2'-bipyridine

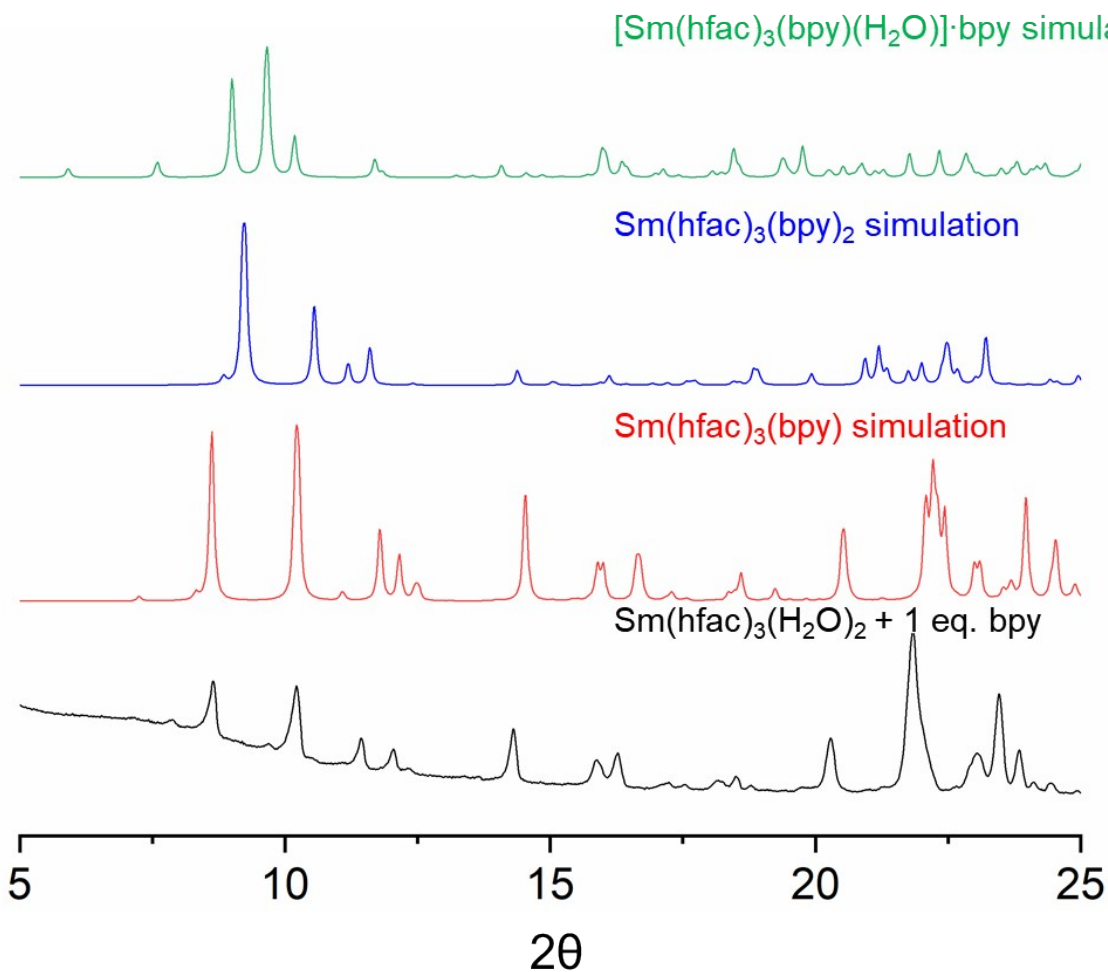


Figure S30. Simulated PXRD spectra of (top) $[\text{Sm}(\text{hfac})_3(\text{bpy})(\text{H}_2\text{O})]\cdot\text{bpy}$, (second from top) $\text{Sm}(\text{hfac})_3(\text{bpy})_2$, (third from top) $\text{Sm}(\text{hfac})_3(\text{bpy})$ obtained from single crystal data collected at 150 K, and (bottom) the PXRD spectrum of crude reaction of $\text{Sm}(\text{hfac})_3(\text{H}_2\text{O})_2$ and 1 eq. of 2,2'-bipyridine

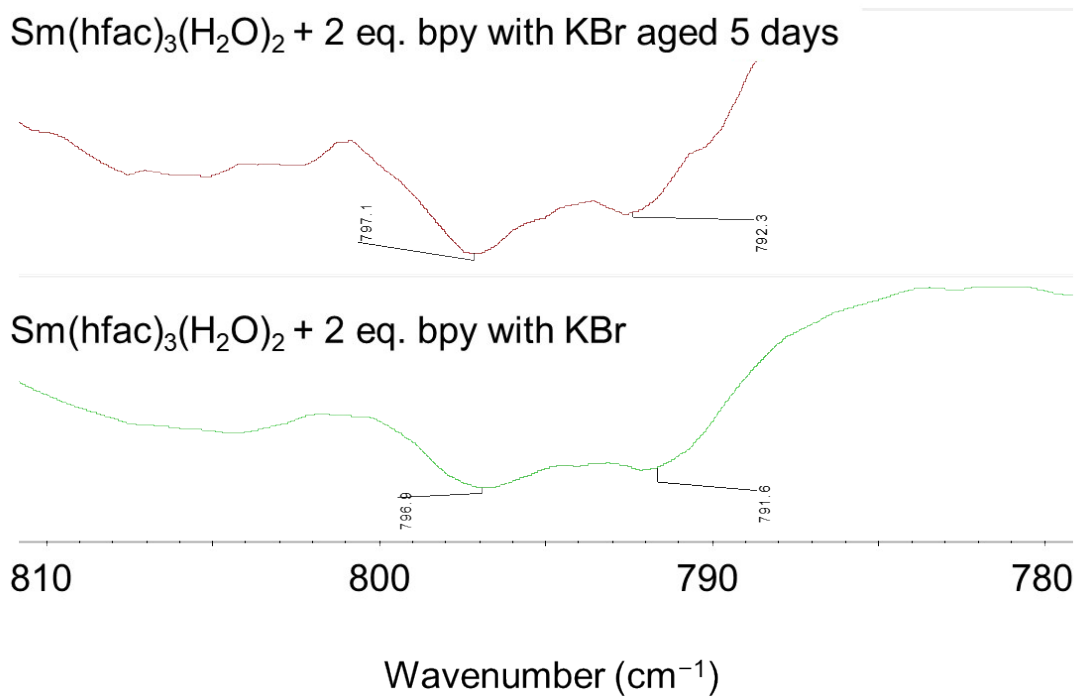


Figure S31. Excerpt from FT-IR spectra of the reaction of (top) Sm(hfac)₃(H₂O)₂ with 2 eq. bpy ground with KBr and aged 5 days, and (bottom) Sm(hfac)₃(H₂O)₂ and 2 eq. bpy ground with KBr after 20 minutes.

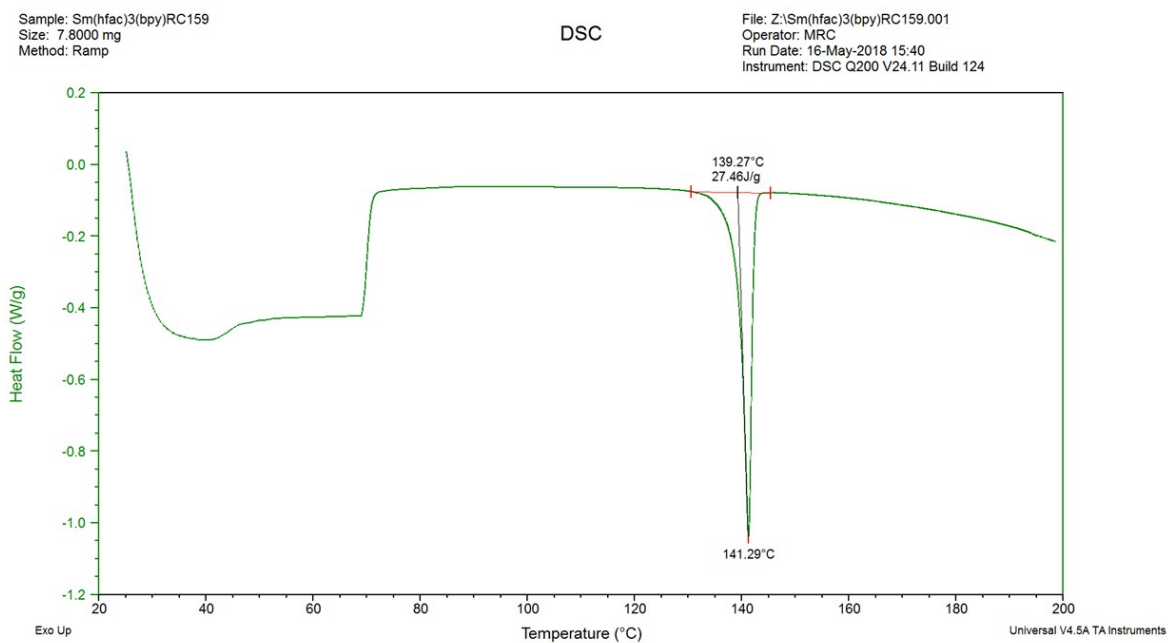


Figure S32. DSC of crude material from mechanochemical reaction of Sm(hfac)₃(H₂O)₂ and 1 eq. of 2,2'-bipyridine ($T_i = 25$ °C heating 25 °C/min to 70 °C, heating 5 °C/min from 70 °C to 200 °C)

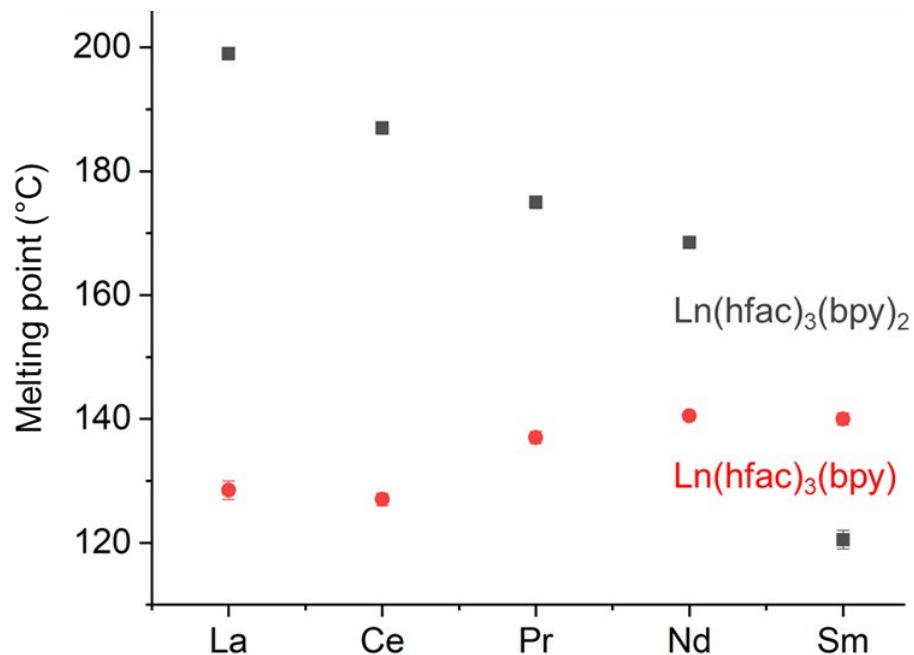


Figure S33. Trend in melting points obtained for pure 8-coordinate Ln(hfac)₃(bpy) complexes and 10-coordinate Ln(hfac)₃(bpy)₂ complexes

Table S1: Trends in Ln-N bond length and N-Ln-N bond angle of 8-coordinate Ln(hfac)₃(bpy) complexes

	Ln-N (Å)	Ln-N _{avg} (Å)	N-Ln-N (°)	N-Ln-N _{avg}
La	2.640 2.653 2.659 2.680	2.658	60.98 60.93	60.96
Ce	2.62 2.644 2.627 2.629	2.63	61.31 61.89	61.60
Pr	2.611 2.627 2.608 2.606	2.613	61.68 62.10	61.89
Nd	2.600 2.575 2.577 2.592	2.586	62.45 62.70	62.58
Sm	2.535 2.545 2.562 2.544	2.544	63.81 63.22	63.52

Table S2: Assignment of Coordination Geometries of 8-coordinate Ln(hfac)₃(bpy) Complexes from Haight's Method¹ using the 16th, 17th and 18th smallest angles

Selected angle	Angle (°)	Assigned Geometry ^a	Selected Angle	Angle (°)	Assigned Geometry ^a
O25-La1-O31	84.10	Square antiprism (20.76°) ^b	O81-La2-O91	85.68	Square antiprism (21.69°)
N1-La1-O45	104.86		N62-La2-O95	107.37	
N12-La1-O41	116.21		N51-La2-O91	112.64	
O25-Ce1-O31	84.20	Square antiprism (21.06°)	O81-Ce2-O91	84.28	Square antiprism (23.64°)
N1-Ce1-O45	105.26		N62-Ce2-O95	107.92	
N12-Ce1-O41	116.13		N51-Ce2-O91	114.19	
O25-Pr1-O31	82.44	Square antiprism (23.80°)	O81-Pr2-O91	84.45	Square antiprism (23.49°)
N1-Pr1-O45	106.24		N62-Pr2-O95	107.94	
N12-Pr1-O41	116.36		N51-Pr2-O91	113.89	
O21-Nd1-O41	81.59	Square antiprism (24.81°)	O75-Nd2-O95	84.10	Square antiprism (24.47°)
N11-Nd1-O35	106.40		N62-Nd2-O71	108.57	
N12-Nd1-O31	116.63		N51-Nd2-O75	114.1	
O25-Sm1-O35	83.10	Square antiprism (25.78°)	O75-Sm2-O91	80.76	Square antiprism (26.71°)
N1-Sm1-O31	108.88		N62-Sm2-O85	107.47	
N12-Sm1-O35	115.06		N51-Sm2-O81	116.64	

^a The geometry was assigned by the difference between the 16th and 17th smallest angles as they are all > 20 ° (D_{4d}), and did not fit the criteria for being assigned as bicapped trigonal prism (C_{2v}) or dodecahedron (D_{2d}).

^b The difference between the 16th and 17th angles is close to 20°, therefore, we could say it is slightly distorted towards bicapped trigonal prism geometry (C_{2v}).

Table S3: Trends in Ln-N bond length and N-Ln-N bond angle for 10-coordinate Ln(hfac)₃(bpy)₂ complexes

	Ln-N (Å)	Ln-N _{avg} (Å)	N-Ln-N (°)
La ^a	2.7741 2.7709	2.7725	57.95
Ce	2.744 2.756	2.750	58.33
Pr	2.737 2.745	2.741	58.89
Nd	2.728 2.733	2.731	58.99
Sm	2.713 2.722	2.718	59.32

^a Refcode: EBUXUU²

Table S4: Comparison of Average Bond Lengths of the Ln-O_{DME}³ and Ln-N_{bpy} bonds in the 8-coordinate Ln(hfac)₃(DME) and Ln(hfac)₃(bpy) Complexes

	Ln-O _{DME} ³ (Å)	Ln-N _{bpy} (Å)
La	2.574	2.658
Ce	2.549	2.63
Pr	2.534	2.613
Nd	N/A	2.586
Sm	2.497	2.544

S3. Crystallography

Data for all La, Ce, Pr 8-coordinate and 10-coordinate complexes and Sm(hfac)₃(bpy)₂ were collected at low temperature (150 K) on a Bruker-Nonius Kappa-CCD diffractometer using monochromated Mo-K α radiation ($\lambda = 0.71073 \text{ \AA}$) and were measured using a combination of ϕ scans and ω scans with κ offsets, to fill the Ewald sphere.⁴ The Sm(hfac)₃(bpy) structure was collected at low temperature (150 K) on a Bruker APEX2 area detector diffractometer using APEX2 software using monochromated Mo-K α radiation ($\lambda = 0.71073 \text{ \AA}$). For the Nd complexes, data were collected at low temperature (150 K) on a SuperNova Agilent diffractometer equipped with a microfocus Mo K α radiation ($\lambda = 0.71073 \text{ \AA}$) source and Atlas CCD detector. The unit cell refinement and data reduction were carried out using CrysAlisPro software.

The structures were solved (direct methods) and refined using the programs listed in Table S5 for full-matrix least-squares refinement on F^2 against all reflections. H atoms were included in calculated positions and allowed to refine as riding on their respective carbon atoms.

Table S5. Details of Crystallographic Solutions and Refinement

	Collection	Absorption Correction	Cell Refinement and Reduction	Solution	Refinement
La(hfac) ₃ (bpy)	Bruker Nonius	SORTAV ⁵	DENZO-SMN ⁴	SIR-92 ⁶	SHELXL-2016/6 ⁷
Ce(hfac) ₃ (bpy)	Bruker Nonius	SORTAV ⁵	DENZO-SMN ⁴	SHELXTL V6.1 ⁸	SHELXL-2016/6 ⁷
Pr(hfac) ₃ (bpy)	Bruker Nonius	SORTAV ⁵	DENZO-SMN ⁴	SHELXS-97 ⁸	SHELXL-2016/6 ⁷
Nd(hfac) ₃ (bpy)	Agilent Supernova	SCALE3 ABSPACK ⁹	CrysAlisPro Version 1.171.35.8 ¹⁰	SHELXS-97 ⁸	SHELXL-2016/6 ⁷
Sm(hfac) ₃ (bpy)	Bruker APEX2	SADABS ¹¹	Bruker SMART and Bruker SAINT	SHELXS-97 ⁸	SHELXL-2016/6 ⁷
Ce(hfac) ₃ (bpy) ₂	Bruker Nonius	SORTAV ⁵	DENZO-SMN ⁴	SHELXTL V6.1 ⁸	SHELXL-2016/6 ⁷
Pr(hfac) ₃ (bpy) ₂	Bruker Nonius	SORTAV ⁵	DENZO-SMN ⁴	SHELXTL V6.1 ⁸	SHELXL-2016/6 ⁷
Nd(hfac) ₃ (bpy) ₂	Agilent Supernova	SCALE3 ABSPACK ⁹	CrysAlisPro Version 1.171.35.8 ¹⁰	SHELXS-97 ⁸	SHELXL-2013 ^{7, 12}
Sm(hfac) ₃ (bpy) ₂	Bruker Nonius	SORTAV ⁵	DENZO-SMN ⁴	SHELXTL V6.1 ⁸	SHELXL-2016/6 ⁷

References

1. C. W. Haigh, *Polyhedron*, 1995, **14**, 2871-2878.
2. D. R. Van Staveren, G. van Albada, J. G. Haasnoot, H. Kooijman, A. M. M. Lanfredi, P. J. Nieuwenhuizen, A. L. Spek, F. Ugozzoli, T. Weyhermüller, J. Reedijk, *Inorg. Chim. Acta.*, 2001, **315**, 163-171.
3. E. M. Fatila, E. E. Hetherington, M. Jennings, A. J. Lough, K. E. Preuss, *Dalton Trans.*, 2012, **41**, 1352-1362.
4. Z. Otwinowski and W. Minor, in *Macromolecular Crystallography, Pt A*, eds. C. W. Carter and R. M. Sweet, Academic Press, London, 1997, vol. 276, pp. 307.
5. R. H. Blessing, *Acta Crystallogr., Sect. A: Found Crystallogr.*, 1995, **51**, 33.
6. A. Altomare, G. Cascarano, C. Giacovazzo, A. Guagliardi, M. C. Burla, G. Polidori and M. Camalli, *J. Appl. Crystallogr.*, 1994, **27**, 435.
7. G. M. Sheldrick, *Acta Crystallogr., Sect. C: Struct. Chem.*, 2015, **71**, 3.

8. G. M. Sheldrick, *Acta Crystallogr., Sect. A: Found. Crystallogr.*, 2008, **64**, 112.
9. Empirical absorption correction using spherical harmonics, implemented in SCALE3 ABSPACK scaling algorithm. Agilent Technologies, Xcalibur CCD system, CrysAlisPro Software System; Version 1.171.35.8. 2011
10. Agilent Technologies, Xcalibur CCD system, CrysAlisPro Software System; Version 1.171.35.8. 2011.
11. G. M. Sheldrick, SADABS. Program for Empirical Absorption Correction University of Gottingen, Germany, 1996.
12. T. Gruene, H. W. Hahn, A. V. Luebben, F. Meilleur and G. M. Sheldrick, *J. Appl. Crystallogr.*, 2014, **47**, 462.